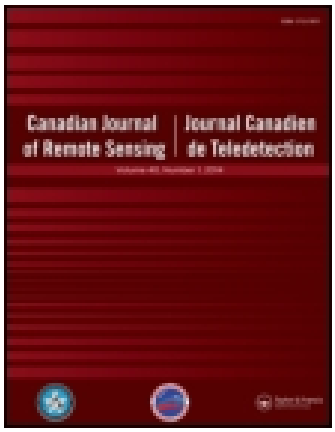

Canadian Journal of Remote Sensing: Journal canadien de télédétection
Publication details, including instructions for authors and subscription information:
http://www.tandfonline.com/loi/ujrs20

Testing a vehicle-based scanning lidar sensor for crop detection

J. Selbeck, V. Dworak & D. Ehlert
Published online: 02 Jun 2014.

To cite this article: J. Selbeck, V. Dworak & D. Ehlert (2010) Testing a vehicle-based scanning lidar sensor for crop detection, Canadian Journal of Remote Sensing: Journal canadien de télédétection, 36:1, 24-35, DOI: 10.5589/m10-022

To link to this article: http://dx.doi.org/10.5589/m10-022

Can. J. Remote Sensing, Vol. 36, No. 1, pp. 24–35, 2010

Testing a vehicle-based scanning lidar sensor for crop detection

J. Selbeck, V. Dworak, and D. Ehlert

Abstract. Light detection and ranging (lidar) systems are widely used in space, airborne, and terrestrial applications. In agriculture, lidar systems have the potential to gather crop stand parameters. Taking these parameters into consideration, crop production processes such as fertilizing, crop protection, and harvesting can be optimized in real time. The vehicle-based use of lidar technology in agriculture for collecting such parameters is in the initial stage of research and development. This paper investigates a vehicle-based laser scanner system with respect to its measuring properties in maize stands and discusses measurement errors caused by the laser beam shape, laser layer, laser echoes, angle of view, and variable data density and their elimination probabilities. The scanner data were used to generate a three-dimensional (3D) model. The height and volume calculated from the model correlate with the weighted biomass. Furthermore, the results show a velocity independence over a wide speed range. The validation of these values demonstrates the high robustness of this sensor.

Résumé. Les systèmes lidar sont utilisés couramment dans les applications spatiales, aéroportées et terrestres. En agriculture, les systèmes lidar ont la capacité d'acquérir des informations sur les paramètres des cultures. En prenant en considération ces différents paramètres, il est possible d'optimiser en temps réel les processus de production des cultures tels que la fertilisation, la protection des cultures et les récoltes. L'utilisation de la technologie lidar en agriculture à partir d'un véhicule pour l'acquisition de tels paramètres en est présentement à ses débuts aux plans de la recherche et du développement. On étudie dans cet article un système de scanneur laser embarqué sur véhicule pour déterminer ses capacités de mesure dans le cas des cultures du maïs. On discute des erreurs de mesure causées par la forme du faisceau laser, la couche laser, les échos laser, l'angle de visée ainsi que la densité variable des données et de leurs probabilités d'élimination. Les données du scanneur ont été utilisées pour générer un modèle 3D. La hauteur et le volume calculés à partir du modèle sont corrélés avec la biomasse mesurée. De plus, les résultats montrent une indépendance par rapport à la vélocité pour une grande diversité de vitesses. La validation de ces valeurs démontre la grande robustesse de ce capteur. [Traduit par la Rédaction]

Introduction

About 50% of the total available land surface in Europe is used for agricultural production, with about 53% in Germany (Maul et al., 2008). Most of the crops have to be cultivated and harvested each year. In contrast with forest trees, agricultural crops have a very short life cycle and therefore a high growth dynamic. Crops grow to ripeness stage within a few weeks. Repeated operations for fertilizing and crop protection are necessary during this growing season.

Crop stand parameters, such as crop height, degree of coverage, crop stand volume, and biomass, are all important for the assessment of crops in agricultural production processes. These parameters can be used to appraise the expected crop yield and optimize the fertilizer and pesticide quantities for site-specific crop management. Furthermore, parameters such as ground speed or the rotation speed of functional units (rasp-bar cylinder, cutter head) can be adapted to site-specific crop conditions in harvesting combines (Ehlert et al., 2007).

Spectral measuring methods are presented in the literature to detect crop vegetation indexes (Pinter et al., 2003). For this purpose, space, airborne, and terrestrial photographs and multispectral scanner images with different wavelengths or rather colors, including red, green, and near-infrared wavebands, were taken to calculate, for example, the normalized difference vegetation index (NDVI) (Antolin et al., 2008; Morsdorf et al., 2008; Arroyo et al., 2008; Waser et al., 2008). These methods are suitable for characterizing crop parameters such as biomass and photosynthetic activity mainly in early growth stages (Inman et al., 2008), but not during the ripeness time of crops when the chlorophyll decreases to zero, such as in wheat. Moreover, no information about the structural properties of crop stands can be gathered by this method.

Spaceborne laser scanner systems are available for detecting wide swaths of land via satellite (Doraiswamy

Received 8 October 2009. Accepted 22 January 2010. Published on the Web at http://pubservices.nrc-cnrc.ca/cjrs on 10 September 2010.

J. Selbeck,[1] V. Dworak, and D. Ehlert. Leibniz Institute for Agricultural Engineering Potsdam-Bornim (ATB), Max-Eyth-Allee 100, 14469 Potsdam, Germany.

[1]Corresponding author (e-mail: jselbeck@atb-potsdam.de).

et al., 2003; Karjalainen et al., 2008), and airborne scanner systems (Senay et al., 2000) are available for detecting medium-range areas from aircraft (500–1000 m) and helicopters (200–300 m) (Baltsavias, 1999a; 1999b; Wehr and Lohr, 1999). These very cost intensive technologies (>€500 000) are mainly used for remote sensing of large-scale landscapes (Hopkinson et al., 2006; Wu et al., 2006; Roth and Thompson, 2008; Goepfert et al., 2008) and urban areas (Vu et al., 2003) and in forestry (Devereux et al., 2008; Wang et al., 2008). Terrestrial laser scanner (TLS) systems are suitable for surveying purposes, cultural heritage, city modeling, or architectural applications (Dold and Brenner, 2008); for mobile road mapping systems (Graefe, 2008); and for the determination of forest inventory parameters (Bienert et al., 2006; Danson et al., 2008). These systems cost €50 000 or more.

Buildings, the surface of landscapes, and trees also usually have large dimensions and show marginal changes over long periods of time. To manage agricultural crop production, current information is needed in time, and sometimes within a matter of hours or even seconds. Therefore, many agricultural vehicles should be equipped with a low-cost sensor to perform online operations. The sensor systems described earlier are unacceptable for agricultural applications due to the very high investment costs and the delayed data delivery. The spot diameters of lasers used in airborne and terrestrial remote sensing of trees are decimetres or greater.

In agriculture, it is necessary to measure from and in front of moving vehicles such as tractors or self-propelled machines. Furthermore, agricultural objects such as leaves, stems, and soil surfaces have very individual shapes and different surface angles related to the laser beam direction and can also have small dimensions compared with those of the laser beam. Characteristic examples for these conditions are measurements in grass and cereals, which have a highly complex structure. Analyzing the reflection signals (full waveform) provides more detailed and improved information about the target objects (Bretar et al., 2008; Neuenschwander, 2008; Wagner et al., 2004; 2008). Low-cost sensors do not offer this option of full waveform analysis. Under these conditions, it is not known how to assess the readings gathered from more simple sensors in cases where one laser shot hits different ranged crops or the soil surfaces because of the mismatch between the laser beam diameter and the filigree of grass leaves.

From the aspect of beam guidance, it is possible to distinguish between sensors with a fixed beam and those with a scanning beam. Existing laser scanners provide the user with limited opportunities to influence the movement of the beam. Individual solutions can be developed for lasers with a fixed beam by moving the entire sensor housing with the appropriate kinematics (Ehlert et al., 2007).

In the field of agricultural research, market-available low-cost laser rangefinders have been explored. Thösink et al. (2004) made a first test to measure the height of oat plants using a triangulation rangefinder, and in a comparative study Kirk et al. (2004) estimated the canopy structure from laser range measurements and computer vision. Ehsani and Lang (2002) used a laser scanner to estimate the volume of geometric objects with a defined shape (cylinders) and of soybean plants under laboratory conditions. Ehlert et al. (2008) measured crop biomass density by laser triangulation in oilseed rape, winter rye, winter wheat, and grassland, and Lenaerts et al. (2008) predicted crop plant density using lidar sensors.

Ehlert et al. (2007) assessed low-cost laser rangefinders with small beam diameters (fixed-beam type) for vehicle-based measuring of crop biomass. High functional correlations were found between mean reflection height h_{Rmean} (in metres), calculated from the measured reflection range and sensor height, and fresh crop biomass density FMD (in kg/m^2). The quality of fit for a linear regression was more than 0.90 ($R^2 > 0.9$) for crops, namely oilseed rape, winter rye, and winter wheat. The accuracy was lower in grassland (pasture) because of the occurrence of several plant species with variable morphology and the small dimensions of the leaves and stems (**Table 1**).

In the measurements in this study, the beam was directed down into the plants or was pivoted around a horizontal axis of $\pm 15^{\circ}$. The mounting height of the sensor, and thus the measuring range, was less than 2.5 m. Under these conditions, the diameter of the laser beam was in the range of about 7 mm. The arrangement of measuring points followed either a straight line or a sinusoidal line with an amplitude of less than 1.34 m.

Lenaerts et al. (2008) tested two lidar sensors for predicting crop stand density under laboratory conditions. The sensors were mounted at a height of 2.85 m on a combine harvester. Lenaerts et al. concluded that a sufficient measuring distance and a small beam diameter

Table 1. Coefficients of determination for the relationship between crop biomass density and mean reflection height for small ranges <2.50 m (Ehlert et al. 2007).

		No. of plots		Regression equation		R^2	
Crop cultivar	Growth stages	LASE sensor	Acuity sensor	LASE sensor	Acuity sensor	LASE sensor	Acuity sensor
Oilseed rape	51–61	8	8	$h_{\mathrm{Rmean}} = 0.090\mathrm{FMD}$	$h_{\mathrm{Rmean}} = 0.077\mathrm{FMD}$	0.92	0.97
Winter rye	31–69	13	13	$h_{\mathrm{Rmean}} = 0.146\mathrm{FMD}$	$h_{\mathrm{Rmean}} = 0.116\mathrm{FMD}$	0.91	0.90
Winter wheat	30–59	10	10	$h_{\mathrm{Rmean}} = 0.091\mathrm{FMD}$	$h_{\mathrm{Rmean}} = 0.074\mathrm{FMD}$	0.94	0.96
Grassland	—	8	8	$h_{\mathrm{Rmean}} = 0.153\mathrm{FMD}$	$h_{\mathrm{Rmean}} = 0.099\mathrm{FMD}$	0.61	0.48

are necessary to prevent failure of the measurements caused by spots larger than the target objects and by striking edges of objects.

Agricultural equipment for applications involving fertilizers and plant protection agents normally has a working width greater than 20 m. Today, high-end combine harvesters can reach cutting widths in the range of 10 m. The measurements must be performed on a broader strip in front of the machines to acquire plants in a representative manner for these working widths. Because of these higher ranges, beam divergence is more crucial and leads to the problems described previously. Owing to these operational demands, laser rangefinders must survey crop parameters from up to a distance of about 15 m. No experience with crop stands currently exist for this measurement range. In a first step, a suitable (market-available) laser rangefinder with increased measuring potential had to be found and arranged on a basic agricultural vehicle (tractor).

The main objectives of this article are to (*i*) investigate the measurement properties of a chosen laser rangefinder in crop stands and (*ii*) process the sensor readings for crop stand characterization.

Material and methods

Selection of a suitable (market-available) laser rangefinder

The laser rangefinder sensors used in previous scientific investigations were assessed to measure crop stand parameters over short ranges. From the point of view of the authors, these sensors did not meet the requirements to be able to work on vehicles under field conditions. Therefore, a prerequisite for testing the measuring potential of laser rangefinders in crop production was to find a suitable sensor model. Based on an analysis of market-available laser rangefinders, a laser scanner developed for automobile driver assistance functions (ibeo ALASCA XT, Automobile Sensor GmbH, Hamburg, Germany; price €69 000) was chosen (**Figure 1**).

The ALASCA laser scanner is an instrument based on lidar technology and measures the time of flight of the pulse. The built-in laser has a wavelength of 905 nm and generates short, rapid-fire pulses, which are transmitted into the environment by a tilted rotating mirror. The reflected laser pulse of a target is recorded in terms of intensity by a photodiode inside the scanner. If the intensity falls below a threshold, the measured value is discarded. The laser scanner transmits and analyses up to four echo pulses for different target distances over a period of one measurement pulse. This lidar device has the potential to measure the depth of the crop stand and almost completely eliminates disturbance sources such as raindrops and dust. Furthermore, the sensor has four layers that have an angle of divergence of 0.8° between each layer. In an automobile driver assistance system, the four layers are used to securely detect obstacles, at different heights above the base level (street) or even if the vehicle makes some pitching motions. A single beam has a divergence of 0.8° in the vertical direction and 0.08° in the horizontal direction (according to the user's manual). These lead to a 4 × 4 matrix as shown in **Table 2**.

Figure 1. Photograph of the ibeo ALASCA XT laser scanner.

The sensor can work with different mirror rotation frequencies of from 8.0 to 40.0 Hz and different resolutions depending on the rotation frequency. The chosen frequency of 12.5 Hz provides the highest combination of frequency and resolution, with angular resolutions of 0.25° for $\gamma < \pm 16°$, 0.50° for $\gamma = \pm 16°$ to $\pm 60°$, and 1.00° for $\gamma = \pm 60°$ to $\pm 90°$ (where γ is the scan angle used in the scan plane; **Figure 3**). When the laser beam hits a target, the scanner displays x' and y' coordinates via the Ethernet connection.

Arrangement of the sensor on a basic agricultural vehicle (tractor)

As described previously, the laser scanner had to be mounted on a basic vehicle to simulate the measuring condition on a forage harvester for maize harvesting. We used an available tractor because a forage harvester is a very expensive and heavy machine. To simulate the position of the scanner on the cabin of the forage harvester, the tractor was equipped with a mounting frame (**Figure 2**; equalizer bars are not mounted).

The frame made it possible to mount the scanner at a height of 3.7 m (Z_S) above the ground and thus higher than

Table 2. Layer–echo matrix of the ALASCA XT laser scanner.

		Echo pulse			
Layer	Channel	1st	2nd	3rd	4th
4	Green (top)	4A	4B	4C	4D
3	Blue	3A	3B	3C	3D
2	Yellow	2A	2B	2C	2D
1	Red (bottom)	1A	1B	1C	1D

Figure 2. Principle setup of the measurements in maize.

the maize stand. In this case, the laser scanner was mounted with an angle $\varphi = 61^\circ$ to the Z axis (see **Figure 3**). In this arrangement, the tilt of 61° ensures that the laser beam does not hit the vehicle, with the exception of the tractor exhaust pipe. **Figure 3** shows a schematic of the setup. The sensor is fix-mounted, so the measurements may be defective if the vehicle experiences longitudinal or transversal tilt movements. The moving direction is equal to the X axis, and the scan direction to the Y axis. The angle γ remains as the scan angle, and the coordinates x'_S ,y'_S are the echo positions of the sight of the scanner. Each x'_S ,y'_S point must be transformed to the new X–Y–Z coordinates using the following equations:

$$Y = y'_S \tag{1}$$

$$X = x'_S \sin(\varphi) \tag{2}$$

$$Z = Z_S - x'_S \cos(\varphi) \tag{3}$$

The angle $\varphi = 61^\circ$ represents the neutral plane between scan layers 2 and 3. Starting from this, four different angles φ_1–φ_4 were used ($\varphi_1 = 59.8^\circ$, $\varphi_2 = 60.6^\circ$, $\varphi_3 = 61.4^\circ$, and $\varphi_4 = 62.2^\circ$) for the transformation of the individual layers. **Figure 4a** shows the data for one typical original scan line from a maize stand measured with the laser scanner, and **Figure 4b** shows the useful transformed Z heights from **Figure 4a**. The original x'_S ,y'_S data from the scanner only represent simple distance information, but after the transformation the new X–Y–Z data are descriptive because the defined mounting height of the scanner provides a reference to the ground level.

Investigation procedure

The investigation took place during the maize harvest season in 2008. Accessibility to maize plots with different yields was given by the chosen harvested area. To investigate the measuring properties of the laser scanner, 10 randomly selected areas (named plots Maize1 to Maize10) were scanned. **Figure 2** shows a typical maize stand, which illustrates that the individual plants stay very close to one another and the leaves typically overlap. As a result of the overlay and the lack of analogue echo signals, the echo signals of the laser scanner cannot be correlated with local parameters of the sample, which is possible for the scientific lidar systems in remote sensing (Wagner et al., 2003). The measurements were taken at an almost constant vehicle speed (about 0.9 km/h). After the datalogging was

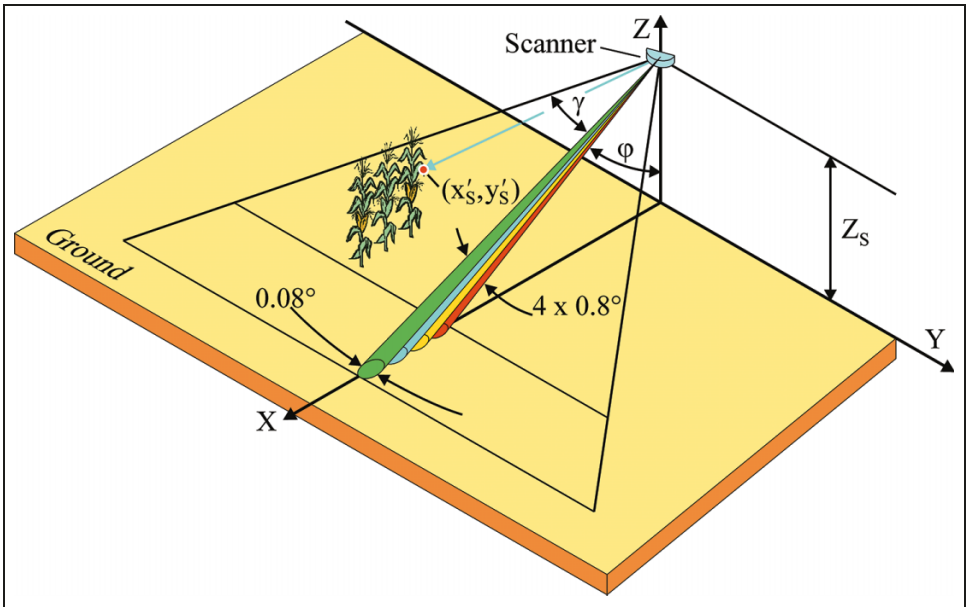

Figure 3. Schematic of the setup.

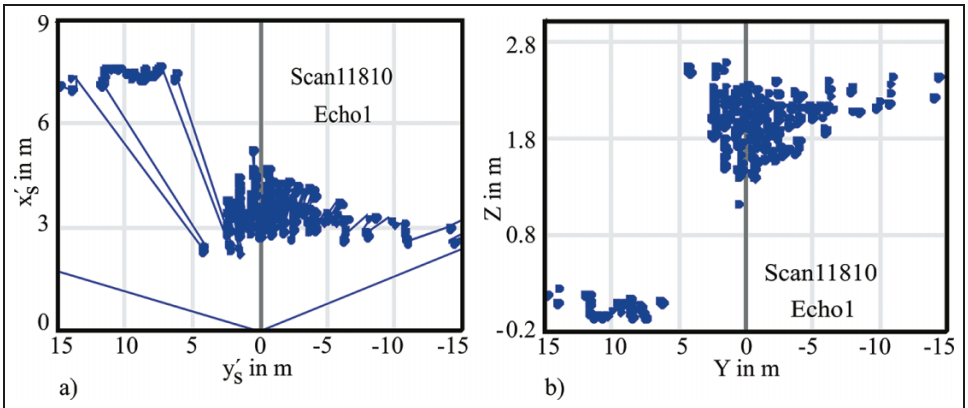

Figure 4. (a) Example of a typical scan line with the original x'_S, y'_S data for the first echo coordinate. (b) Transformed height Z versus direction Y data.

started, the vehicle was accelerated to the measurement speed and reached the area of interest.

The original scanner data were transferred to the PC via the Ethernet connection. The given file format of the scanner was interpreted with a self-written C-program and stored on a hard disk. The data were imported to the Microsoft Excel program via a Visual Basic for Applications macro. In Excel, the x'_S,y'_S data were then transformed to X–Y–Z data including the given angle and the vehicle speed from the experiment. These data were then imported to the SAS Institute Inc. (2004) program for the statistical calculations and then to the ARCView GIS 3.2 program for visualization of the three-dimensional (3D) point clouds (ESRI, 1999). Numerous parameters are given or can be calculated from the point cloud data: M is the mean value of the reflection heights, e.g., point heights in the stand without the ground values ($Z > 0.3$ m); and P95 and P99 are the height percentiles at 95% and 99% of the point heights without the ground values ($Z > 0.3$ m).

Results

The readings from plot Maize1 are used as an example to characterize the measuring properties of this setup. **Figures 5–8** show the 3D point clouds of Layer2 from the first area of the stand Maize1 from echo signals Echo1–Echo4. This includes the histogram of the reflection height and the number of points. The projection planes for the Z–X and Z–Y directions are presented. The left side of the Z–X projection shows the beginning of the crop stand, and the Z–Y projection shows the view of the maize plant rows. **Figure 5** displays the Echo1 point cloud and its histogram, which is a Gaussian-shaped profile around the mean level of the reflection height. A second peak is noticeable at the zero level. This peak is induced by the ground hits caused by the start-up in front of the stand corner. In such a high stand density, just a few ground hits for Echo1 (i.e., the first echo) are visible after the beginning of the crop stand. In the stand, only a small peak in the histogram for the ground level is typical for the Echo1 of this laser scanner. The Z–Y projection for the Echo1 point cloud is displayed on the right side in **Figure 5**, which shows that the number of maize plant rows can be counted. **Figure 6** displays the associated Echo2 data. Higher order echoes always represent inner hits in the stand. The distribution is very different from the Echo1 distribution. First, the number of echoes is much smaller. Second, the histogram shows two mean peaks. Third, Echo2 has plenty of ground hits; as expected, it should be possible to use Echo2 for an independent ground level calibration. **Figure 7** depicts the associated Echo3. The

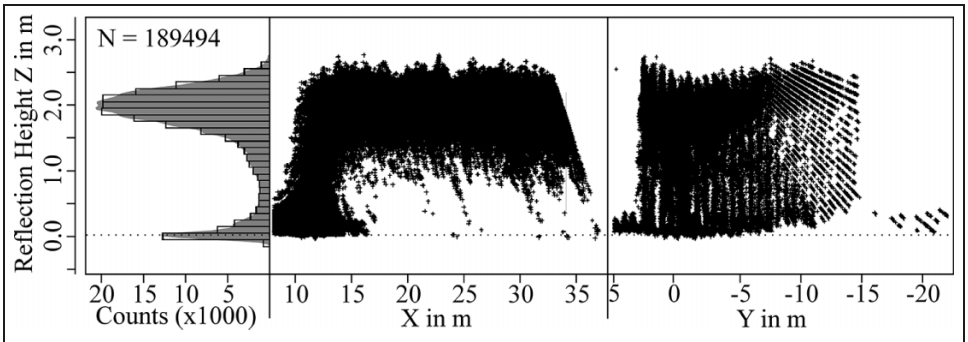

Figure 5. Laser beam hit distribution of Layer2–Echo1 in the Maize1 measurement (histogram, distribution in X direction and Y direction).

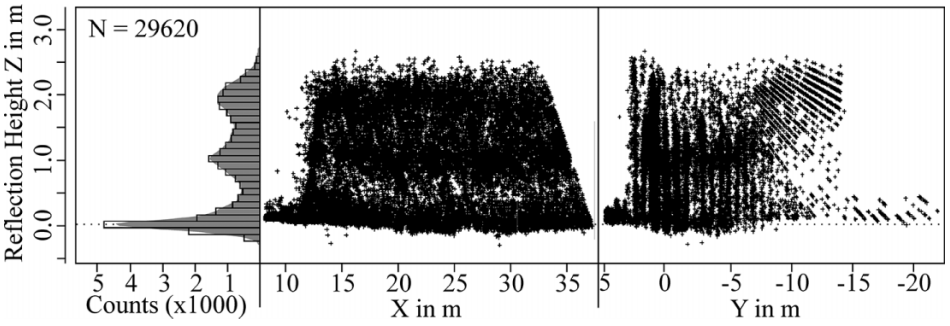

Figure 6. Laser beam hit distribution of Layer2–Echo2 in the Maize1 measurement (histogram, distribution in *X* direction and *Y* direction).

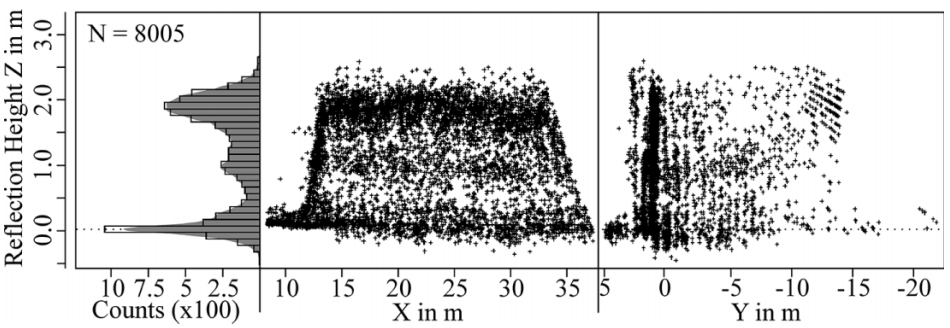

Figure 7. Laser beam hit distribution of Layer2–Echo3 in the Maize1 measurement (histogram, distribution in *X* direction and *Y* direction).

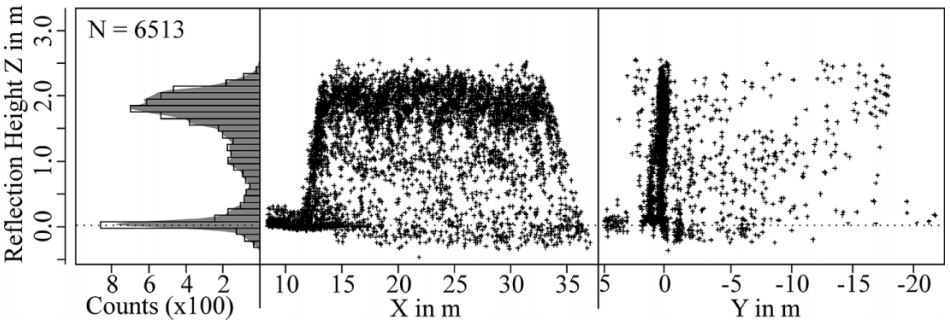

Figure 8. Laser beam hit distribution of Layer2–Echo4 in the Maize1 measurement (histogram, distribution in *X* direction and *Y* direction).

number of points is continuously reduced, and the histogram is different from the others. The highest concentration is located directly under the scanner position (**Figure 7**, right image). This tendency is even more obvious for the Echo4 concentration in **Figure 8**.

The 3D visualization of point clouds, such as Echo1 in **Figure 9**, demonstrates how well an observer can connect the data to the actual situation in the maize stand. From a technical point of view, it is important to generate parameters that are useful for improving the operation of harvesters. **Figure 10** shows the associated P99 value of the maize stand. A 0.75 m × 0.75 m grid pattern was thus overlaid at ground level to calculate the local P99 values. This grid size is used because of the 0.75 m distance between the maize rows. The grid is adjusted such that the maize row is at the midpoint in the grid. In the mean regions, there are typically 700 data points in a 0.75 m × 0.75 m single pad. The P99 value corresponds approximately to the surface of the maize stand. The local volume can be calculated based on the knowledge of the ground level. For this example, an overall volume of 986 m^3 is calculated, and the footprint of the stand is about 427 m^2. Therefore, the mean volume per square metre is 2.3 m^3. **Figures 5–8** show that all four echoes have a ground-level correlation with the theoretical zero value for the ground given by the setup (see **Figure 3**). However, all echoes are influenced by the plant character-

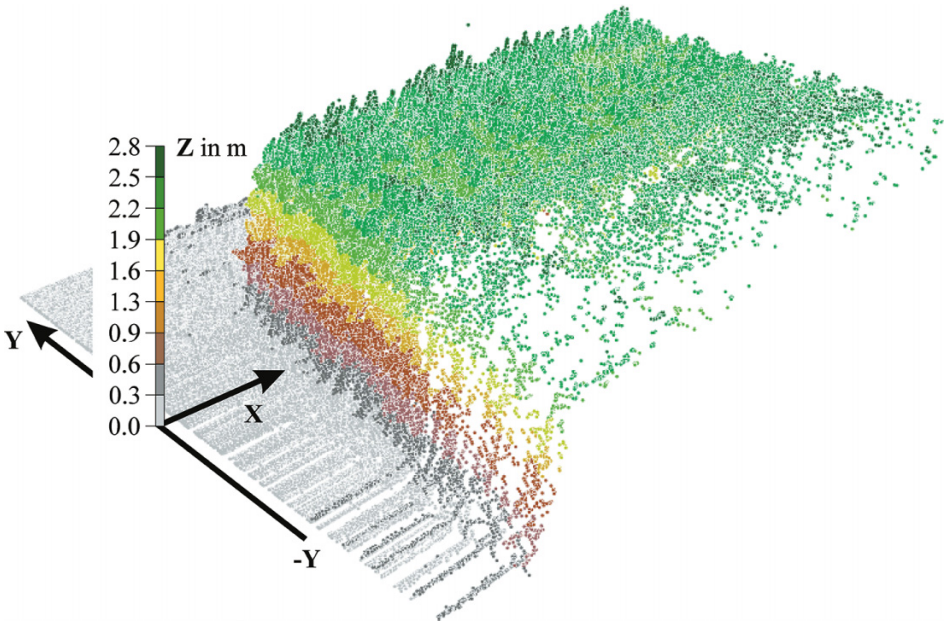

Figure 9. Displayed point cloud data from Maize1, Layer2, Echo1.

istics. The ground-level hits from Echo1 will vary with variations in the plant density. Echo3 and Echo4 have far fewer hits. Echo2 will even vary with the density, but the number of ground hits is significantly greater than the number of plant hits.

More important is the biomass prediction for harvesters. **Figure 11** shows the ratio of the measured biomass versus reflection height. The 10 different biomass data points are real measured maize weights from the 10 different scan areas from plots Maize1 to Maize10. The power trend line is used because an additional constraint can be made for the zero cross point; the biomass has to be zero if the height measurement is zero. The trend line fits the measured data with a correlation of $r^2 = 0.94$.

As already stated, the scanner measures four independent layers simultaneously. The local difference between the P99 values from Layer1, Echo1 and Layer2, Echo1 are displayed in **Figure 12**. The small scaling of the Z axis in a range of 0.3 m helps in visualizing the small difference between the two measurements. Two results emerge from the difference

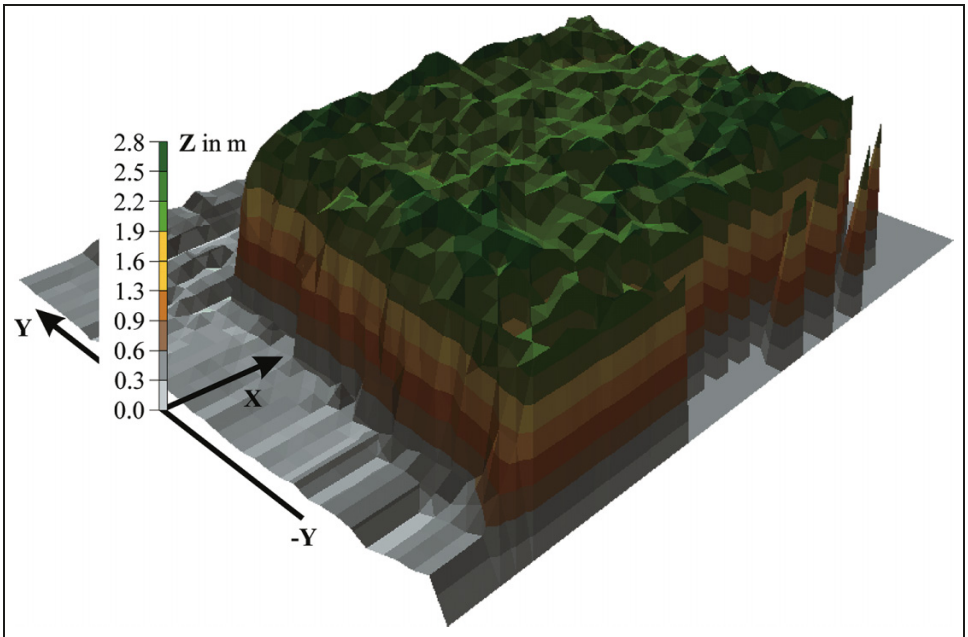

Figure 10. P99 values from Maize1, Layer2, Echo1.

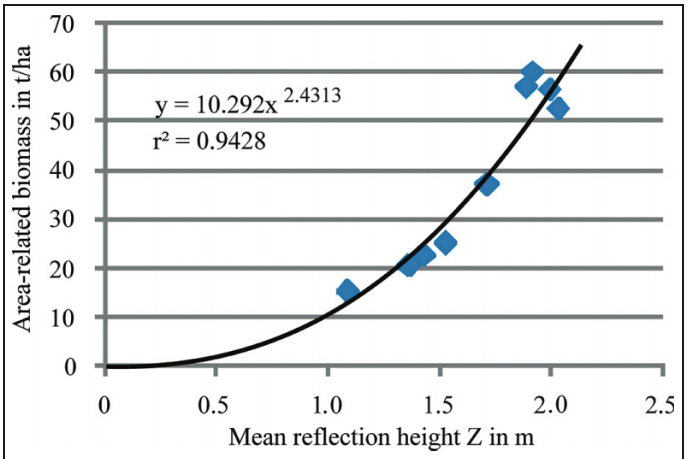

Figure 11. Biomass versus reflection height distribution with a power trend line.

between the layers. First, there is always a positive difference (see **Table 3**). This is caused by the different angle φ between the four layers. As φ increases, the larger distance and angle generate a larger laser spot diameter. The convolution of the larger spot diameter and the crop stand induce higher measurement levels. Ehlert et al. (2008) showed the effect on other crops. Because of the angle dependence, the stand always looks taller when measured with a high scan angle γ in the outer off-axis region (see, therefore, **Figures 5** and **10**). Because the spot diameter increases with an increase in the working distance, the calculated height difference between the layers is always greater for the measured ground levels than for the stand values (**Figure 12**). Second, the small variations in the difference signal (after subtraction of the systematic offset) demonstrate the high reliability of the setup. The effective angle difference between the layers becomes smaller for greater scan angles γ. The error level (or better offset level) in the off-axis region of the difference plot (**Figure 12**) becomes smaller, corresponding to the smaller effective angle difference. **Table 3** presents the differences (mean modulus, not necessarily always positive) between the layers from the P99 values and the mean values *M*. This table includes the difference values from the ground and stand data. These values explain the larger offset for the ground level, due to the greater working distance, as mentioned previously.

With a more detailed view of **Figure 10**, a tendency for taller crops is visible for the off-axis region. This systematic height error is caused by the scan angles γ and the effective incidence angle, which increase in the off-axis region. The effect is generated by the convolution of the laser spot with the crops and the angle-dependent shift of the distribution in the histogram. Caused by the internal scanner setup, the elliptical spot shape is always oriented in the *x*-direction for its long axis. Owing to the growing scan angle γ, the projected long elliptical axis rotated out of the viewing direction and the height effect is reduced. Depending on the working distance, the incident angle (depends on angles φ and γ), and the rotation of the elliptical beam shape (depends on angle γ), the previously described height effect influences each measurement point in the 3D room differently. This effect should be determined for realistic measurements in different maize stands, and thus 10 different maize stands with homogeneous stand elevation were analyzed. The point values were averaged in the *x* direction within 1 m sections in the *y* direction. **Figure 13** shows the results for the P99 values, the mean values from all maize stands, and the resulting linear regression.

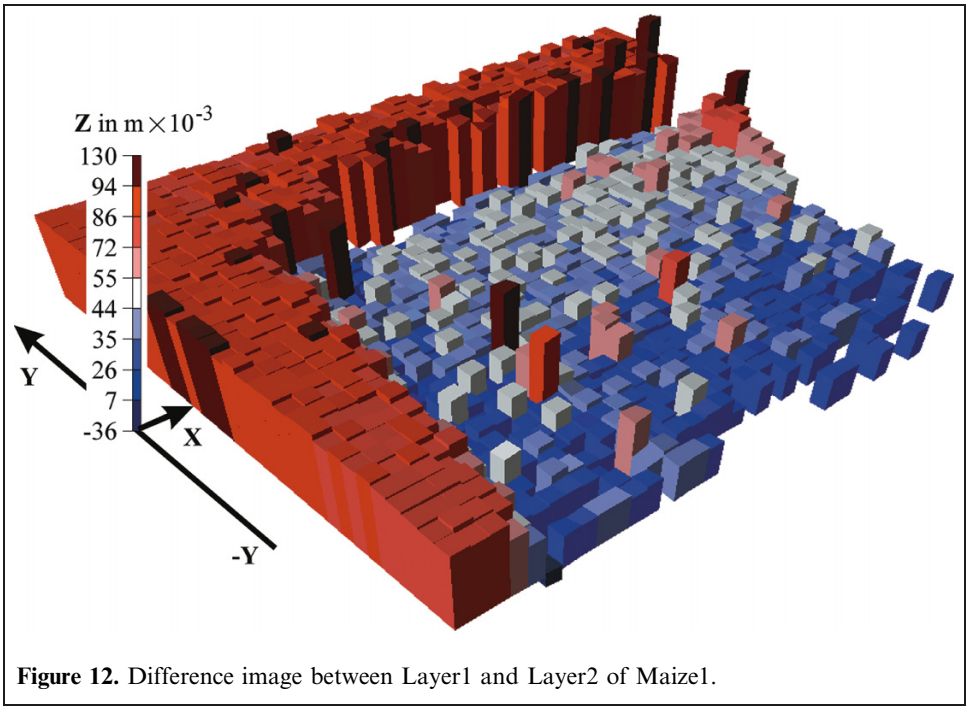

Figure 12. Difference image between Layer1 and Layer2 of Maize1.

Table 3. Differences of mean and P99 values between all layers and their standard deviations (in m × 10^{-3}).

(A) Mean

	Layer1			Layer2			Layer3		
Echo1	M_S	M_G	M_M	M_S	M_G	M_M	M_S	M_G	M_M
Layer2	39.3 ± 9.1	88.2 ± 5.1	57.0 ± 26.0						
Layer3	78.2 ± 14.8	176.8 ± 10.1	114.0 ± 52.0	38.9 ± 7.8	88.9 ± 7.8	57.0 ± 27.0			
Layer4	117.5 ± 21.1	266.3 ± 13.1	171.0 ± 78.0	78.2 ± 14.2	178.4 ± 10.6	11.5 ± 53.0	39.3 ± 8.2	89.5 ± 4.2	58.0 ± 28.0

(B) P99

	Layer1			Layer2			Layer3		
Echo1	$P99_S$	$P99_G$	$P99_M$	$P99_S$	$P99_G$	$P99_M$	$P99_S$	$P99_G$	$P99_M$
Layer2	31.6 ± 16.2	85.3 ± 16.4	51.0 ± 37.0						
Layer3	62.6 ± 19.5	170.2 ± 25.3	101.0 ± 63.0	31.0 ± 9.6	85.7 ± 19.6	51.0 ± 35.0			
Layer4	94.2 ± 26.9	255.1 ± 29.2	153.0 ± 87.0	62.6 ± 20.0	170.6 ± 24.1	103.0 ± 60.0	31.6 ± 16.5	85.0 ± 11.7	52.0 ± 33.0

Note: M_G, mean of ground; M_M, mean overall; M_S, mean value in stand; $P99_G$, percentile 99% of ground; $P99_M$, percentile 99% overall; $P99_S$, percentile 99% value in stand.

To analyze the resolution for separating individual crops in the stand, the setup was analyzed with the measurement shown in **Figure 14**. Because the individual maize lines can be separated in the *y* direction, a 0.5 m thick piece of point cloud in the middle of one maize line was analyzed. The point cloud data were supplemented with high-resolution (each 100 mm in the *x* direction was averaged) P99 and P95 values and the mean *M*.

Neither the point cloud nor the P99 values can discriminate individual crops, which means that the resolution of the laser scanner is probably not high enough or the overlapping maize or its shape is not applicable for detecting individual maize plants. Therefore, no automated rating or disease detection can be performed.

Of course, the point cloud density is very high. Therefore, the system should have a statistically high robustness, which suggests that the vehicle speed could be raised. Speeds higher than 20 km/h are not reasonable in an agricultural area. The multiplication of the vehicle speed of 0.9 km/h as used in the study by 32 results in a speed of 28.8 km/h. This would be analogous to the use of the data from every 32nd scan line to calculate the mean and percentile values. To eliminate the effects of statistical outliers, the calculations were made several times with an offset of four scan lines, e.g., 0, 32, 64, 96, etc. for the first data block, 4, 36, 68, 100, etc. for the second data block, and so on. The result is detailed in **Figure 15**.

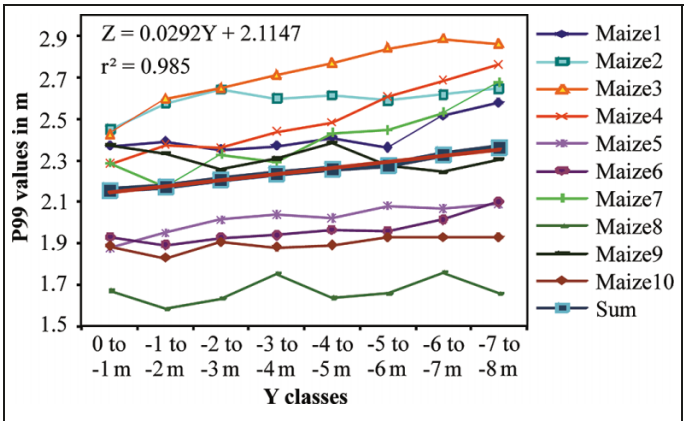

Figure 13. Stand-averaged P99 levels depending on the off-axis region for 10 different maize stands. Both the mean values and the linear regression with $Z = 0.0292Y + 2.1147$ m and $r^2 = 0.985$ are included.

Discussion

The ALASCA XT laser scanner was designed for use in the automotive industry. Its beam divergence (14 mrad × 1.4 mrad) is much higher in one direction than that for typical lidar sensors (0.2–2.0 mrad for remote sensing; Wagner et al., 2003). However, with the short working distance of 2–40 m, the results show explanatory point clouds, which can be interpreted to provide more detailed information about crop stands (**Figure 9**). The histogram shape (**Figure 5**) suggests that the data from the point clouds can be allocated by statistical methods. The local percentile value of 99% (**Figure 10**) can be used to generate the surface

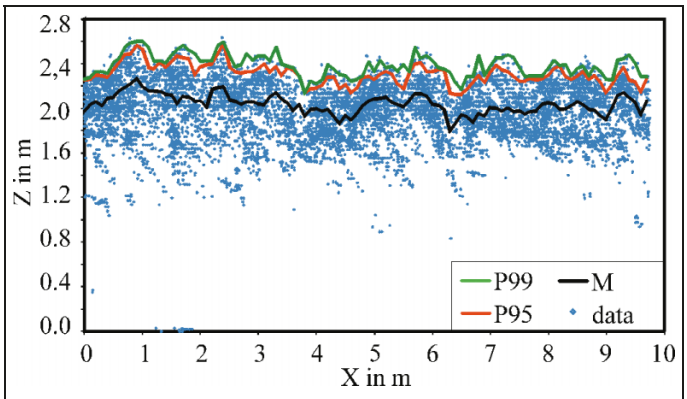

Figure 14. Point cloud data from one maize line with a thickness of 0.5 m (Layer2, Echo1).

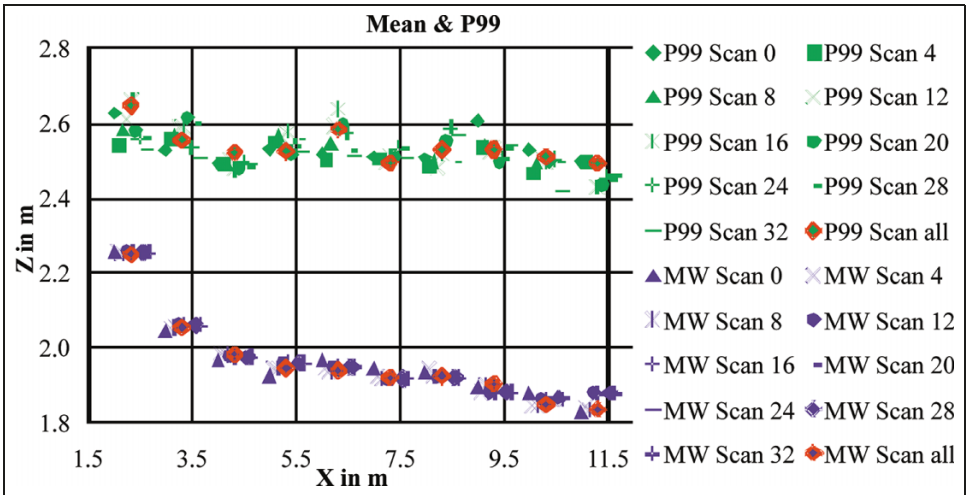

Figure 15. Display of the statistical robustness of the scanner data by comparison of the original data and reduced data. P99 results are displayed in the upper scatterplot, and the mean (MW) results in the lower scatterplot.

plot of a maize stand and accordingly the local volume and biomass. The reflection height or volume versus biomass diagram (**Figure 11**) shows the correlation with the power trend line. The higher variability of the upper values can be explained by an additional corncob on taller plants and fewer leaves per plant because the lower leaves are often senescent and die back for higher plants. The volume and biomass information is usable as the first-order approach to control the harvester ground speed, for example. As the infield measurements show, ground-level results from the Echo2 signals (**Figure 6**) correlate with the theoretical ground level defined by the mounting height of the scanner. Because of the incident angle of the setup, ground hits always differ from the x position of stand hits in a single scan. Errors generated by vibration and tilting of the vehicle thus cause incorrect ground information for the associated stand information at the same x position. Therefore, an extra local ground-level correction does not provide any additional advantage. In any case, the errors do not dominate the results. This is visible by means of the sharp peak in the ground-level histogram in **Figure 6**. The higher order echoes indicate the possibility of the laser beam interfusing the maize stand. Certainly, it should be taken into account that higher order echoes depend on the scan angle γ (**Figures 7** and **8**).

The high repeatability of this measurement principle was estimated by the small differences (**Table 3**) between the local P99 values from the four independent layers. As described previously, the large beam divergence induces errors in the reflection height information. Nevertheless, small variations in the mounting angle φ only generate an offset for the in-stand data. As long as the setup is not changed, a unique level calibration should provide sufficient results in practice. The standard deviation in a range of a few millimetres between the four different measured layers demonstrates the high repeatability of the setup. Furthermore, with a high scan angle γ, the beam divergence induces errors in the averaged reflection height for the off-axis data. The formula effort to describe the amplifying and reducing parameters is enormous and can be reduced to a simple linear approach for limited scan angles γ.

The large mounting angle of $\varphi = 61^\circ$ gives the possibility of generating point cloud data in front of a harvester, for example, and allocating control information with a sufficient lead time. Each layer generates 350 16-bit data tuples at a rate of 12.5 times per second plus one global positioning system (GPS) dataset per second, which is less than 18 kilobytes of data per second.

The disadvantage is that the resolution is limited by the large working distance and the beam shape. Saeys et al. (2009) introduce the "field reconstruction" method for crop density estimation. They were able to demonstrate that counting the number of wheat ears per square metre is possible after data processing of their high-resolution scanner data. Although individual maize lines can be separated with our setup, no single maize plant can be detected (**Figure 14**). Therefore, the field reconstruction is not possible for maize with the system being used. Nevertheless, this is not really a drawback for maize stand analyses because the diameter of maize is in the range of half a metre and the drilling distance is 0.1 m. Even a smaller sensor mounting angle φ cannot lead to separating the maize because of the typical overlay in the range of 80%.

The huge overlay and the point cloud scanner data, however, induce solid surface information. Even the use of every 32nd scan line provides reasonable statistical results for the stand volume, which confirms the high robustness of the setup. As a result, the vehicle speed could be increased or the amount of data for data processing could be reduced to save computer resources.

Conclusions

A vehicle-based light detection and ranging (lidar) sensor offers many benefits for generating different control parameters for agricultural machines. In contrast with other applications, in-field vehicle-based sensors must be dust-proof, waterproof, and vibration-proof. Furthermore, they must be inexpensive. Just one of these requirements eliminates most existing lidar sensors from being used on agricultural machinery such as harvesters, spreaders, and sprayers.

As the results have demonstrated, the ALASCA XT sensor gives sufficient surface information about maize stands to calculate the volume and biomass parameters for controlling machines. Some measurement inaccuracies exist, but they are understandable and can be first-order eliminated with a single calibration in most cases. Even a variation in data density can be neglected in the range of typical harvester velocities. The usability for other crops should be investigated in future tests. Taking into account that the follow-up model of this sensor (the ibeo-LUX sensor) is much more compact and less expensive (currently about €12 000 but, according to manufacturer information, about €1000 once it has been introduced as standard equipment in the automotive sector), there is the potential for the use of lidar technology in agriculture.

References

Antolín, R., Calzado-Martínez, C., Gómez, A., Manzanera, J.A., Meroño, J.E., Pedrazzani, D., Pérez, H.H., Roldán-Zamarrón, A., Santos, I., and Valbuena, R. 2008. LINHE Project: development of new protocols for the integration of digital cameras and LiDAR, NIR and Hyperspectral sensors. In *SilviLaser 2008: Proceedings of the 8th International Conference on LiDAR Applications in Forest Assessment and Inventory*, 17–19 September 2008, Edinburgh, UK. Edited by R.A. Hill, J. Rosette, and J. Suarez. CD-ROM. Forestry Commission, Edinburgh, UK. pp. 355–364.

Arroyo, L.A., Johansen, K., Armston, J., Phinn, S., and Pascual, C. 2008. Integration of LiDAR and QuickBird imagery for mapping riparian zones in Australian tropical savannas. In *SilviLaser 2008: Proceedings of the 8th International Conference on LiDAR Applications in Forest Assessment and Inventory*, 17–19 September 2008, Edinburgh, UK. Edited by R.A. Hill, J. Rosette, and J. Suarez. CD-ROM. Forestry Commission, Edinburgh, UK. pp. 113–122.

Baltsavias, E.P. 1999a. Airborne laser scanning: existing systems and firms and other resources. *ISPRS Journal of Photogrammetry and Remote Sensing*, Vol. 54, No. 2–3, pp. 164–198.

Baltsavias, E.P. 1999b. Airborne laser scanning: basic relations and formulas. *ISPRS Journal of Photogrammetry and Remote Sensing*, Vol. 54, No. 2–3, pp. 199–214.

Bienert, A., Scheller, S., Kesane, E., Mullooly, G., and Mohan, F. 2006. Application of terrestrial laser scanners for the determination of forest inventory parameters. In *Proceedings of the ISPRS Commission V Symposium*, 25–27 September 2006, Dresden, Germany. Edited by H.G. Maas and D. Schneider. ITC, Enschede, The Netherlands. International Archives of Photogrammetry, Remote Sensing and Spatial Information Sciences, Vol. 36, Part 5.

Bretar, F., Chauvea, A., Mallet, C., and Jutzi, B. 2008. Managing full waveform LIDAR data: A challenging task for the forthcoming years. In *Proceedings of the 21st ISPRS Congress, Commission I*, 3–11 July 2008, Beijing. ITC, Enschede, The Netherlands. International Archives of Photogrammetry, Remote Sensing and Spatial Information Sciences, Vol. 37, Part B1, pp. 415–420.

Danson, F.M., Armitage, R.P., Bandugula, V., Ramirez, F.A., Tate, N.J., Tansey, K.J., and Tegzes, T. 2008. Terrestrial laser scanners to measure forest canopy gap fraction. In *SilviLaser 2008: Proceedings of the 8th International Conference on LiDAR Applications in Forest Assessment and Inventory*, 17–19 September 2008, Edinburgh, UK. Edited by R.A. Hill, J. Rosette, and J. Suarez. CD-ROM. Forestry Commission, Edinburgh, UK. pp. 335–341.

Devereux, B.J., Amable, G.S., Liadsky, J., and Crow, P. 2008. Small footprint, full waveform LiDAR modelling of canopy 3D structure in complex, semi-natural woodland communities. In *SilviLaser 2008: Proceedings of the 8th International Conference on LiDAR Applications in Forest Assessment and Inventory*, 17–19 September 2008, Edinburgh, UK. Edited by R.A. Hill, J. Rosette, and J. Suarez. CD-ROM. Forestry Commission, Edinburgh, UK. p. 386.

Dold, C., and Brenner, C. 2008. Analysis of score functions for the automatic registration of terrestrial laser scans. In *Proceedings of the 21st ISPRS Congress, Commission V*, 3–11 July 2008, Beijing. ITC, Enschede, The Netherlands. International Archives of the Photogrammetry, Remote Sensing and Spatial Information Sciences, Vol. 37, Part B5, pp. 417–422.

Doraiswamy, P.C., Moulin, S., Cook, P.W., and Stern, A. 2003. Crop yield assessment from remote sensing. *Photogrammetric Engineering & Remote Sensing*, Vol. 69, No. 6, pp. 665–674.

Ehlert, D., Adamek, R., and Horn, H.-J. 2007. Assessment of laser rangefinder principles for measuring crop biomass. In *Precision Agriculture '07: Proceedings of the 6th European Conference on Precision Agriculture*, 3–6 June 2007, Skiathos, Greece. J.V. Stafford. Wageningen Academic Publishers, Wageningen, The Netherlands. pp. 317–324.

Ehlert, D., Horn, H.-J., and Adamek, R. 2008. Measuring crop biomass density by laser triangulation. *Computers and Electronics in Agriculture*, Vol. 61, pp. 117–125.

Ehsani, R., and Lang, L. 2002. A sensor for rapid estimation of plant biomass. In *Proceedings of the 6th International Conference on Precision Agriculture*, 14–17 July 2002, Minneapolis, Minn. Edited by P.C. Robert, R.H. Rust, and W.E. Larson. ASA, CSSA, and SSSA, Madison, Wisc. pp. 950–957.

ESRI. 1999. *ArcView GIS version 3.2*. Environmental Systems Research Institute, Inc. (ESRI), Redlands, Calif.

Goepfert, J., Soergel, U., and Brzank, A. 2008. Integration of intensity information and echo distribution in the filtering process of LIDAR data in vegetated areas. In *SilviLaser 2008: Proceedings of the 8th International Conference on LiDAR Applications in Forest Assessment and Inventory*, 17–19 September 2008, Edinburgh, UK. Edited by R.A. Hill, J. Rosette, and J. Suarez. CD-ROM. Forestry Commission, Edinburgh, UK. pp. 417–426.

Graefe, G. 2008. High precision kinematic surveying with laser scanners. *Journal of Applied Geodesy*, Vol. 1, No. 4, pp. 185–199.

Hopkinson, C., Chasmer, L., Lim, K., Treitz, P., and Creed, I. 2006. Towards a universal lidar canopy height indicator. *Canadian Journal of Remote Sensing*, Vol. 32, No. 2, pp. 139–152.

Inman, D., Khosla, R., Reich, R., and Westfall, D.G. 2008. Normalized difference vegetation index and soil color-based management zones in irrigated maize. *Agronomy Journal*, Vol. 100, No. 1, pp. 60–66.

Karjalainen, M., Kaartinen, H., and Hyyppä, J. 2008. Agricultural monitoring using Envisat alternating polarization SAR images. *Photogrammetric Engineering & Remote Sensing*, Vol. 74, No. 1, pp. 117–126.

Kirk, K., Thomson, A., and Anderson, H.J. 2004. Estimation of canopy structure from laser range measurements and computer vision: A comparative study. In *AgENG2004, Proceedings of the International Conference on Agricultural Engineering*, 12–16 September 2004, Leuven, Belgium. Edited by J. De Baerdemaaker. Technological Institute, Leuven, Belgium. Book of Abstracts, pp. 420–421.

Lenaerts, B., Craessaerts, G., De Baerdemaeker, J., and Saeys, W. 2008. Crop stand density prediction using LIDAR sensors. In *AgENG2008, Proceedings of the International Conference on Agricultural Engineering*, 23–25 June 2008, Hersonissos, Crete, Greece. European Society of Agricultural Engineers, Bedford, UK. OP 390.

Maul, A.G., Richter, M., and Gramm, U. 2008. *Statistisches Jahrbuch über Ernährung Landwirtschaft und Forsten 2008*. Wirtschaftsverlag NW GmbH, Bremerhaven, Germany.

Morsdorf, F., Nichol, C., Malthus, T.J., Patenaude, G., and Woodhouse, I.H. 2008. Modelling multi-spectral LIDAR vegetation backscatter — assessing structural and physiological information content. In *SilviLaser 2008: Proceedings of the 8th International Conference on LiDAR Applications in Forest Assessment and Inventory*, 17–19 September 2008, Edinburgh, UK. Edited by R.A. Hill, J. Rosette, and J. Suarez. CD-ROM. Forestry Commission, Edinburgh, UK. pp. 257–265.

Neuenschwander, A.L. 2008. Evaluation of waveform deconvolution and decomposition retrieval algorithms for ICESat/GLAS data. *Canadian Journal of Remote Sensing*, Vol. 34, No. S2, pp. S240–S246.

Pinter, P.J., JrHatfield, J.L., Schepers, J.S., Barnes, E.M., Moran, M.S., Daughtry, C.S.T., and Upchurch, D.R. 2003. Remote sensing for crop management. *Photogrammetric Engineering & Remote Sensing*, Vol. 69, No. 6, pp. 647–664.

Roth, R.B., and Thompson, J. 2008. Practical application of multiple pulse in air (MPIA) LIDAR in large area surveys. In *Proceedings of the 21st ISPRS Congress, Commission I*, 3–11 July 2008, Beijing. ITC, Enschede, The Netherlands. International Archives of Photogrammetry, Remote Sensing and Spatial Information Sciences, Vol. 37, Part B1, pp. 183–188.

Saeys, W., Lenaerts, B., Craessaerts, G., and De Baerdemaeker, J. 2009. Estimation of the crop density of small grains using LiDAR sensors. *Biosystems Engineering*, Vol. 102, pp. 22–30.

SAS Institute Inc. 2004. *SAS OnlineDoc® 9.1.3*. SAS Institute Inc., Cary, N.C.

Senay, G.B., Lyon, J.G., Ward, A.D., and Nokes, S.E. 2000. Using high spatial resolution multispectral data to classify corn and soybean crops. *Photogrammetric Engineering & Remote Sensing*, Vol. 66, No. 3, pp. 319–327.

Thösink, G., Preckwinkel, J., Linz, A., Ruckelshausen, A., and Marquering, J. 2004. Optoelektronisches Sensorsystem zur Messung der Pflanzenbestandesdichte [Optoelectronic sensor system for crop density measurement]. *Landtechnik*, Vol. 59, pp. 78–79.

Vu, T.T., Tokunaga, M., and Yamazaki, F. 2003. Wavelet-based extraction of building features from airborne laser scanner data. *Canadian Journal of Remote Sensing*, Vol. 29, No. 6, pp. 783–791.

Wagner, W., Horn, A.U., and Briese, C. 2003. Der Laserstrahl und seine Interaktion mit der Erdoberfläche [The laser beam and its interaction with the earth surface]. *VGI — Österreichische Zeitschrift für Vermessung und Geoinformation* (4).

Wagner, W., Ullrich, A., Melzer, T., Briese, C., and Kraus, K. 2004. From single-pulse to full-waveform airborne laser scanners: Potential and practical challenges. In *Proceedings of the 20th ISPRS Congress Commission III*, 12–13 July 2004, Istanbul, Turkey. ITC, Enschede, The Netherlands. International Society for Photogrammetry and Remote Sensing, Vol. 35, Part B/3, p. 6.

Wagner, W., Hollaus, M., Briese, C., and Ducic, V. 2008. 3D vegetation mapping using small-footprint full-waveform airborne laser scanners. *International Journal of Remote Sensing*, Vol. 29, No. 5, pp. 1433–1452.

Wang, Y., Weinacker, H., and Koch, B. 2008. A lidar point cloud based procedure for vertical canopy structure analyses and 3D single tree modelling in forest. *Sensors*, Vol. 8, pp. 3938–3951.

Waser, L.T., Ginzler, C., Kuechler, M., and Baltsavias, E. 2008. Potential and limits of extraction of forest attributes by fusion of medium point density LiDAR data with ADS40 and RC30 images. In *SilviLaser 2008: Proceedings of the 8th International Conference on LiDAR Applications in Forest Assessment and Inventory*, 17–19 September 2008, Edinburgh, UK. Edited by R.A. Hill, J. Rosette, and J. Suarez. CD-ROM. Forestry Commission, Edinburgh, UK. pp. 625–634.

Wehr, A., and Lohr, U. 1999. Airborne laser scanning — an introduction and overview. *ISPRS Journal of Photogrammetry and Remote Sensing*, Vol. 54, No. 2–3, pp. 68–82.

Wu, S., Li, J., and Huang, G.H. 2006. Deriving vegetation structure in ecological applications from airborne LiDAR data. *Journal of Environmental Informatics*, Vol. 8, No. 2, pp. 111–115.